THE PLANT CELL

The Plant Cell, 2025, **37**, koae310
https://doi.org/10.1093/plcell/koae310
Advance access publication 21 November 2024
Large-Scale Biology

Quantitative proteomics reveals extensive lysine ubiquitination and transcription factor stability states in Arabidopsis

Gaoyuan Song,[1] Christian Montes,[1] Damilola Olatunji,[2] Shikha Malik,[1] Chonghui Ji,[3] Natalie M. Clark,[1] Yunting Pu,[2] Dior R. Kelley,[2,*] Justin W. Walley[1,*]

[1]Department of Plant Pathology, Entomology, and Microbiology, Iowa State University, Ames, IA 50014, USA
[2]Department of Genetics, Development and Cell Biology, Iowa State University, Ames, IA 50014, USA
[3]Fujian Provincial Key Laboratory of Haixia Applied Plant Systems Biology, Haixia Institute of Science and Technology, Fujian Agriculture and Forestry University, Fuzhou 350002, China
*Author for correspondence: dkelley@iastate.edu (D.K.), jwalley@iastate.edu (J.W.)
The authors responsible for distribution of materials integral to the findings presented in this article in accordance with the policy described in the Instructions for Authors (https://academic.oup.com/plcell/pages/General-Instructions) are: Dior Kelley (dkelley@iastate.edu) and Justin Walley (jwalley@iastate.edu)

Abstract

Protein activity, abundance, and stability can be regulated by post-translational modification including ubiquitination. Ubiquitination is conserved among eukaryotes and plays a central role in modulating cellular function; yet, we lack comprehensive catalogs of proteins that are modified by ubiquitin in plants. In this study, we describe an antibody-based approach to enrich ubiquitinated peptides coupled with isobaric labeling to enable quantification of up to 18-multiplexed samples. This approach identified 17,940 ubiquitinated lysine sites arising from 6,453 proteins from Arabidopsis (*Arabidopsis thaliana*) primary roots, seedlings, and rosette leaves. Gene ontology analysis indicated that ubiquitinated proteins are associated with numerous biological processes including hormone signaling, plant defense, protein homeostasis, and metabolism. We determined ubiquitinated lysine residues that directly regulate the stability of three transcription factors, CRYPTOCHROME-INTERACTING BASIC-HELIX-LOOP-HELIX 1 (CIB1), CIB1 LIKE PROTEIN 2 (CIL2), and SENSITIVE TO PROTON RHIZOTOXICITY1 (STOP1) using in vivo degradation assays. Furthermore, codon mutation of *CIB1* to create a K166R conversion to prevent ubiquitination, via CRISPR/Cas9-derived adenosine base editing, led to an early flowering phenotype and increased expression of *FLOWERING LOCUS T* (*FT*). These comprehensive site-level ubiquitinome profiles provide a wealth of data for future functional studies related to modulation of biological processes mediated by this post-translational modification in plants.

Introduction

Ubiquitin is a well-established post-translational protein modification (PTM) that impacts nearly all aspects of plant biology (Vierstra 2009). Covalent attachment of ubiquitin to substrate proteins occurs in a step-wise fashion involving E1 (ubiquitin activating), E2 (ubiquitin conjugating), and E3 (ubiquitin ligase) enzymes (Kraft et al. 2005; Sadanandom et al. 2012). The attachment of ubiquitin to protein substrates can result in many functional outcomes, including protein degradation or changes in subcellular localization. While ubiquitin is typically attached to lysine residues, it can also be covalently linked to cysteine, serine, threonine, and the amino terminus of target proteins (Abu Hatoum et al. 1998; Ciechanover 2004; Cadwell and Coscoy 2005; Kravtsova-Ivantsiv and Ciechanover 2012; Gilkerson et al. 2015). In addition to positional complexity there is also oligomeric complexity whereby ubiquitin attachments to substrates can occur in various numbers of monomers (Romero-Barrios and Vert 2018). In Arabidopsis, over 1,500 annotated genes are linked to ubiquitin pathways suggesting that the biological processes involving this PTM are extensive (Vierstra 2012). While ubiquitin 26S proteasome (UPS) mediated protein degradation has been demonstrated for most plant hormones (Kelley and Estelle 2012; Tal et al. 2020; Wang et al. 2022), very little is known about the corresponding ubiquitin attachment(s) underlying such regulated proteolysis.

Given the importance of ubiquitin in modulating protein function a range of approaches have been used to identify ubiquitinated proteins in plants. One approach has been to use ubiquitin-associated domains or ubiquitin interaction motifs to affinity purify proteins with ubiquitin conjugates (Maor et al. 2007; Manzano et al. 2008; Igawa et al. 2009). Saracco et al. (2009) developed a transgenic Arabidopsis line containing a 6xHis-UBQ tagged ubiquitin line, which has been used in combination with an additional enrichment step based on the HHR23A ubiquitin binding region (Saracco et al. 2009) or tandem ubiquitin binding entities (Kim et al. 2013; Aguilar-Hernández et al. 2017; Ma et al. 2021) to purify ubiquitinated proteins. These methods are powerful for identifying ubiquitinated proteins but are unable to comprehensively identify the exact amino acid attached to ubiquitin because the enrichment occurs at the protein level. In other eukaryotic systems, the gold standard

Received September 09, 2024. Accepted November 13, 2024

approach uses antibodies that recognize the di-glycine (diGly) remnant of ubiquitin and the ubiquitin-like protein related to ubiquitin protein 1/neuronal precursor cell-expressed developmentally downregulated protein 8 (RUB1/NEDD8), which remains following trypsin digestion, to enrich ubiquitin modified peptides (Kim et al. 2011; Fulzele and Bennett 2018). This diGly antibody enrichment approach has been used on several plant species; yet, the number of identified ubiquitin sites lags behind nonplant studies where >10,000 sites are routinely identified (Li et al. 2015; Xie et al. 2015; Zhang et al. 2017; Chen et al. 2018; Wang et al. 2019b; He et al. 2020; Udeshi et al. 2020; Grubb et al. 2021; Berger et al. 2022). Thus, a combined fractional diagonal chromatography (COFRADIC) approach was developed to identify exact ubiquitin sites and expand our known repertoire of ubiquitinated Arabidopsis proteins (Walton et al. 2016). While COFRADIC has enabled the identification of the largest number of ubiquitin sites (3,009) in Arabidopsis it requires complex in vitro chemical modification and sample processing steps, making it difficult to carry out.

Here, we report a diGly based method, using commercially available antibodies, for quantitative profiling of ubiquitinomes in plants. Our approach utilizes an isobaric tag-based mass spectrometry labeling method that enables sample multiplexing and relative quantification of changes in ubiquitin levels at specific amino acid sites. Isobaric labeling has an advantage over data dependent acquisition (DDA) label-free proteomics approaches in that it does not suffer from missing values between samples, which is a challenge for quantitative studies comparing differences between samples. Using these methods, we report an extensive catalog of ubiquitin attachment sites from Arabidopsis primary root, seedling, and rosette leaves. The identified ubiquitination sites occur on proteins from diverse functional categories and include many well-known 26S ubiquitin proteasome substrates for which the specific modified site was unknown. The ubiquitination sites identified in this study provide a rich resource for future mechanistic studies investigating protein function and deepen our understanding of the Arabidopsis proteome.

Results and discussion

Detection and quantification of ubiquitin-modified proteins in Arabidopsis

Despite widespread interest in protein ubiquitination, the ability to robustly carry out large-scale ubiquitinome analyses remains a challenge. Thus, we sought to expand the catalog of known ubiquitination sites on plant proteins. Toward this aim, we tested several steps in diGly-based ubiquitinome profiling. Alkylation of cysteines is a critical step in proteomic sample preparation and is commonly done using iodoacetamide (IAM). Alkylation conditions are known to impact the frequency of "off target" alkylation of residues other than cysteine. Of particular concern is dialkylation of lysine that mimics the mass shift of diGly-modified lysine (K-ε-GG footprint of K + 114), which was initially reported during in gel peptide digestion (Nielsen et al. 2008). Often chloroacetamide (CAA) is a recommended alternative alkylating reagent. However, several benchmarking studies have found no consistent advantage to using CAA for in solution digestion protocols (Udeshi et al. 2012; Hains and Robinson 2017; Müller and Winter 2017). Additionally, Hains and Robinson (2017) reported high levels of methionine oxidation using CAA relative to IAM. Thus, we sought to compare IAM and CAA off-target alkylation using our typical phenol-filter aided sample preparation (FASP) protein extraction and digestion protocol (Song et al. 2018). For this, extracted proteins were split into six equal aliquots. Three aliquots were alkylated using IAM while the other three were alkylated using CAA. No significant difference in dialkylation between IAM and CAA was observed for any residue (Student's *t*-test, $P < 0.05$) (Fig. 1A). In particular, lysine dialkylation was 0.045% for IAM and 0.051% for CAA (Fig. 1A). Thus, we used IAM for further experiments.

We also tested the capacity of the anti-diGly lysine antibody with the peptides from 10-day-old Arabidopsis (*Arabidopsis thaliana*) seedlings. We applied different amount of input peptides (1, 1.5, 2, 3, and 4 mg) to perform the IP experiments with a fixed amount (0.16 mg) of pan anti-diGly remanent antibody conjugated to agarose beads (PTM Biolabs). One-third of the enriched peptides from each sample were analyzed using a 120 min 1-dimensional reversed phase liquid chromatography gradient to deliver the peptides for tandem mass spectrometry (1D-LC-MS/MS). From these test experiments analyzed using an Orbitrap Exploris 480 mass spectrometer, we identified 1,504.5 to 3,347.5 diGly sites (Fig. 1B), while the diGly peptide enrichment efficiency was from 31.2% to 50.2% (Fig. 1C). These enrichment titrations suggest that a reduced amount, relative to manufactures recommendation, of diGly antibody can be successfully used.

From the 1D-LC-MS/MS runs, we noticed there was a high intensity peak in the total ion current chromatogram (TIC) between the retention time of 60 to 80 min (Supplementary Fig. S1A). Instructing the mass spectrometer to "ignore" high abundance analytes using an exclusion list can increase identification of low abundance peptides. Thus, we created an exclusion list comprised of the most abundant peptides identified in this retention time window (Supplementary Fig. S1B). However, excluding precursors corresponding to these abundant peptides from MS/MS analysis did not result in an increase in ubiquitin sites identification (Supplementary Fig. S1C and D). Thus, we did not use an exclusion list for further experiments.

While label-free approaches are useful for identifying diGly sites, isobaric chemical tags for sample multiplexing offer several advantages for quantifying post-translational modifications (PTMs). Current isobaric tags enable comparisons of up to 18 samples in a single mass spectrometry analysis. As a result, isobaric tag multiplexing improves throughput and significantly minimizes the number of missing peptides quantified across all experimental conditions, which is a major drawback of DDA based label-free analyses. Furthermore, multiplexing facilitates a decrease in the starting material needed, from each sample, for PTM enrichment. Thus, we tested the compatibility of isobaric labeling using tandem mass tags (TMT) (McAlister et al. 2012) with diGly enrichment. In order to investigate the influence of proteasome inhibition as well as ability to detect quantitative differences in ubiquitination, we treated 10-day old Col-0 primary roots with a mock or 100 μM of the 26S proteosome inhibitor bortezomib (BTZ: Gladman et al. 2016) for 3 h. First, we explored TMT labeling followed by diGly enrichment ("TMT -> Enrich" in Fig. 1D). However, despite large-scale enrichment and 2-dimensional (2D) LC-MS/MS this method only recovered 10 potential diGly sites (Supplementary Table S1). This is likely due to TMT labeling the primary amine of the diGly remnant, thereby inhibiting enrichment using the diGly antibody, as has been suggested (Rose et al. 2016; Udeshi et al. 2020).

Next, we tested an alternative approach where we enriched with anti-diGly antibodies and then TMT labeled the immunoprecipitated peptides ("Enrich -> TMT" in Fig. 1D). Excitingly, 2D-LC-MS/MS on a Q Exactive Plus mass spectrometer resulted in quantification of 2,944 diGly-modified lysine residues (Fig. 1E

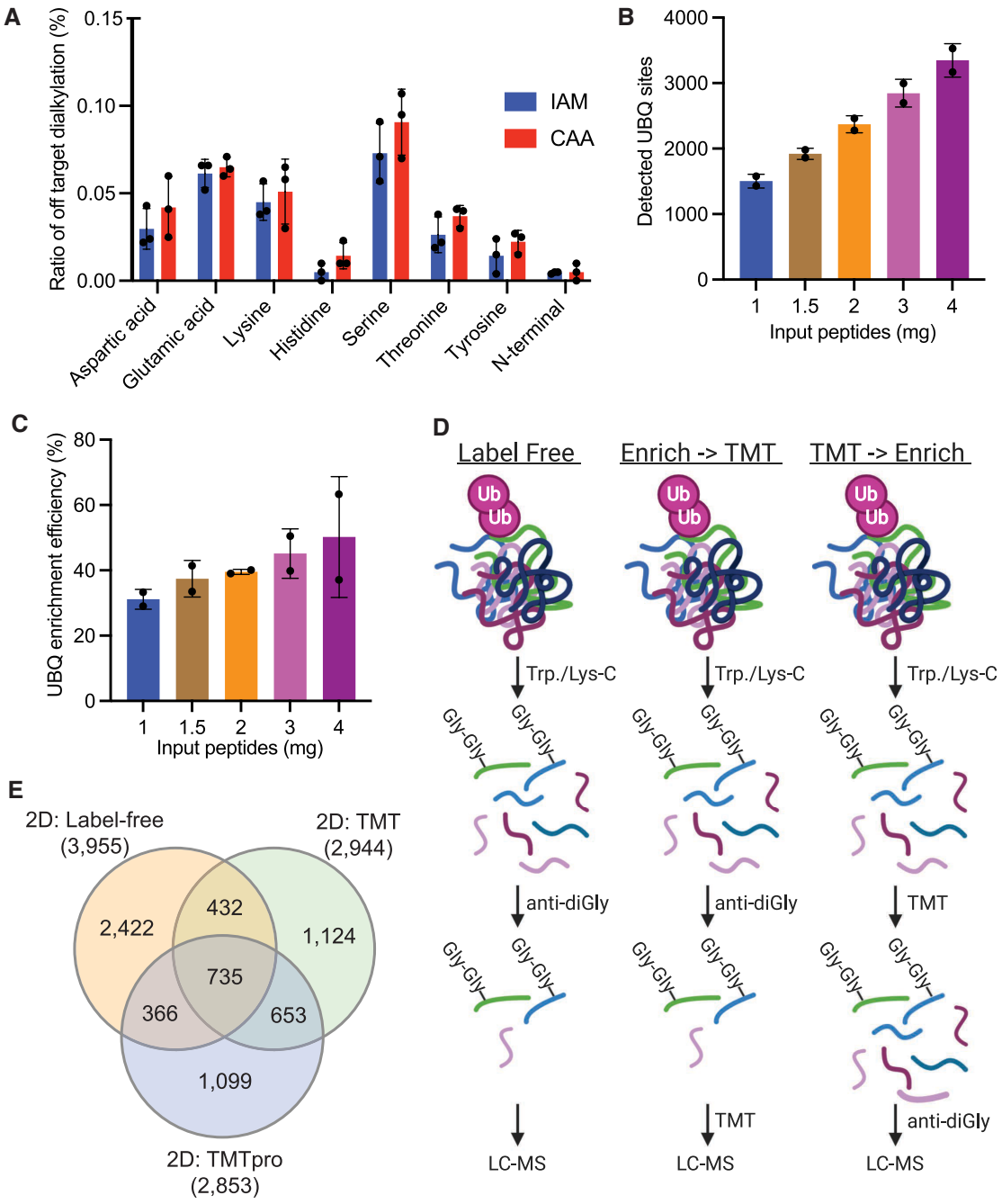

Figure 1. Benchmarking Arabidopsis ubiquitinome profiling methodology. **A)** Percentage of MS2 spectra containing "off target" modification on the specified amino acid following alkylation with either IAM or CAA. Data represent means ± standard deviation (SD) from 3 independent replicates. No statistical differences were observed (Student's *t*-test, $P < 0.05$) **B)** and **C)** Results of the antibody to input peptides ratio. Data represent means ± SD of diGly (UBQ) sites detected by each run **B)** or diGly peptides enrichment efficiency **C)** from 2 independent replicates. **D)** Schematic of workflows tested for quantitative profiling of diGly modified lysine residues. **E)** Overlap in the diGly sites detected using the Label Free and Enrich -> TMT workflows. The Enrich -> TMT approach was tested using both TMT and TMTpro reagents.

and Supplementary Table S1). The original TMT labels used here allowed for multiplexing of up to 11 samples, but a newer TMTpro version was recently developed that can multiplex up to 18 samples. Additionally, TMTpro labels have altered chemical properties and are more hydrophobic compared to TMT 11-plex. Thus, we also tested the newer TMTpro labels for compatibility using an aliquot of the same peptides from the original TMT analysis for diGly enrichment. We were able to quantify a similar (2,853) number of diGly sites using TMTpro multiplexing (Fig. 1E and Supplementary Table S1). Furthermore, the "Enrich -> TMT" method was highly reproducible with average Pearson correlation values between biological replicates of 0.972 and 0.995 for the TMT and TMTpro analyses, respectively. Finally, we performed DDA label-free analysis of the 100 µM BTZ treated roots to compare depth of coverage with TMT multiplexed samples. This large-scale 2D-LC-MS/MS label-free analysis, also on the Q Exactive Plus, resulted in the identification of 3,955 diGly-modified lysine residues. Thus, TMT multiplexing greatly improves throughput while limiting missing values, without dramatically impacting depth of ubiquitin site coverage. Together, these results demonstrate the ability

to analyze plant ubiquitinome using reagents that enable multiplexing, which facilitates large-scale quantitative studies.

Arabidopsis root, seedling, and leaf ubiquitinomes

To expand the scope of the ubiquitinome, we performed additional analysis of seedling and leaf tissues. Specifically, we performed label-free 2D-LC-MS/MS profiling on 100 µM BTZ treated 10-day-old seedling and 3-week-old rosette leaves using an Orbitrap Exploris 480 mass spectrometer. From these samples we identified 10,093 and 8,286 diGly sites from the seedling and leaf tissue, respectively (Fig. 2A and Supplementary Table S2). This demonstrates the utility of this protocol to work across a broad spectrum of vegetative tissues.

To gain insight into the composition of the ubiquitinome we merged the results of all 1D and 2D ubiquitinome experiments we carried out. In total, we identified 17,940 diGly-modified lysine residues sites arising from 6,453 proteins (Fig. 2A and Supplementary Fig. S2 and Table S2). On average, each ubiquitinated protein contained ~2.8 diGly sites. Altogether these data represent a notable increase in the coverage of the Arabidopsis ubiquitinome (Supplementary Table S3).

We used PANTHER to determine enrichment of gene ontology (GO) categories among these 6,453 ubiquitinated proteins (Mi et al. 2019). This analysis uncovered 1,078 enriched GO terms spanning a wide range of biological processes including (de)ubiquitination, transcription, translation, cell wall biogenesis, transport, and lipid metabolism (Fig. 2B and Supplementary Table S4). Additionally, GO terms associated with plant development, growth, and defense were enriched among the ubiquitinated proteins. As a final example, several terms associated with phytohormone pathways including abscisic acid, auxin, brassinosteroid, ethylene, jasmonic acid, and salicylic acid were enriched. This GO analysis highlights the extensive biological functions, which are potentially impacted by ubiquitination and is consistent with the UPS playing a key role in nearly all aspects of plant biology (Vierstra 2009; Kelley and Estelle 2012; Kelley 2018).

A

	Ubiquitin sites	Ubiquitinated proteins
Leaf	8,286	3,656
Root	6,844	3,358
Seedling	13,674	5,329
Total	17,940	6,453

B

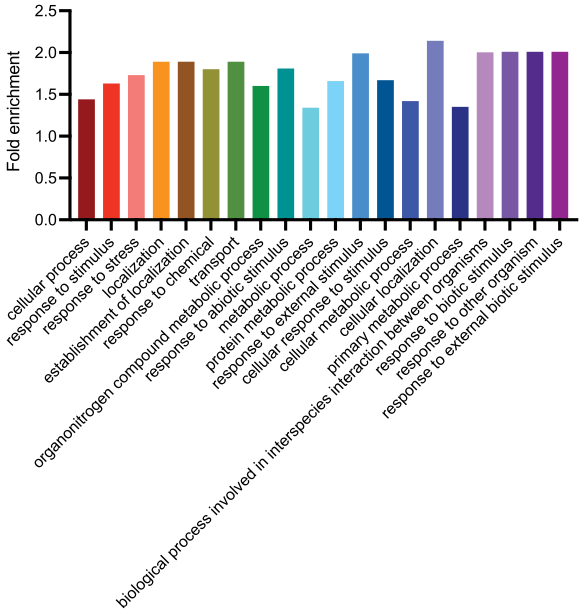

Figure 2. Proteomic analysis of Arabidopsis root, seedling, and leaf ubiquitinomes. **A)** Summary of the Arabidopsis ubiquitinome (i.e. identified ubiquitin sites and ubiquitin proteins). **B)** The top 20 most significantly enriched biological process GO terms of ubiquitinated proteins.

Identification of potential UPS substrates

The attachment of ubiquitin to proteins is known to result in many different functional outcomes including altering protein stability by the UPS. Thus, to identify potential UPS substrates we examined quantitative changes in protein abundance and diGly-modified lysine levels following treatment of primary roots with 100 µM BTZ. For this, we selected Arabidopsis roots because they serve as a key organ for investigating regulation of gene expression and protein turnover via the 26S proteasome has been implicated in regulating root growth and development (Santner and Estelle 2010; Vissenberg et al. 2020). We quantified protein abundance by TMTPro labeling an aliquot of each sample that was used for diGly enrichment and analyzed these "input" samples by 2D-LC-MS/MS (Supplementary Table S5). We first used these data to further examine if our diGly sites may be alkylation artifacts (Nielsen et al. 2008). Despite collecting ~2 times as many MS/MS spectra, in these nonenriched input samples compared to the diGly enriched root samples, we only identified 17 sites with a mass shift matching that of a diGly-modified lysine (K-ϵ-GG footprint of K + 114) (Supplementary Table S6). This is an agreement with the IAM and CAA tests done above (Fig. 1A). Collectively, these experiments demonstrate an extremely low potential false discovery of diGly-modified lysines due to alkylation artifacts and robust identification of in vivo ubiquitin modified sites in our dataset.

Ultimately, we found that 1,336 diGly sites on 691 proteins accumulate following BTZ treatment (Supplementary Table S1). Additionally, we identified 213 proteins increased in abundance following BTZ treatment as potential UPS substrates (Fig. 3A and Supplementary Table S5). To obtain a high-confidence list of UPS substrates, we compared these data with the list of diGly modified proteins and found evidence for 104 proteins as being both diGly modified and exhibiting an increase in protein level following BTZ treatment (Fig. 3A). We examined the PANTHER protein class annotations for these 104 high-confidence UPS candidate proteins and found they are comprised of proteins involved in processes in including transcription and translation, defense, cytoskeleton, and transport (Fig. 3B).

While many of these 104 proteins are previously unreported UPS substrates, several proteins, which are well-established within ubiquitin mediated proteolysis pathways, were observed, including CELL DIVISION CYCLE 48 (CDC48) (Mérai et al. 2014), the transcription factors (TFs) MYC3 (Chico et al. 2020), and AUXIN RESPONSE FACTOR 2 (ARF2) (Walton et al. 2016), the ubiquitin conjugating enzyme UBC34 (Ahn et al. 2018), and the E3 ligase ABI3-INTERACTING PROTEIN 2 (AIP2) (Zhang 2005). These findings confirm previous studies and expand the repertoire of putative 26S proteasome substrates.

We also observed that 343 proteins decreased in abundance following BTZ treatment and that 86 of these proteins were

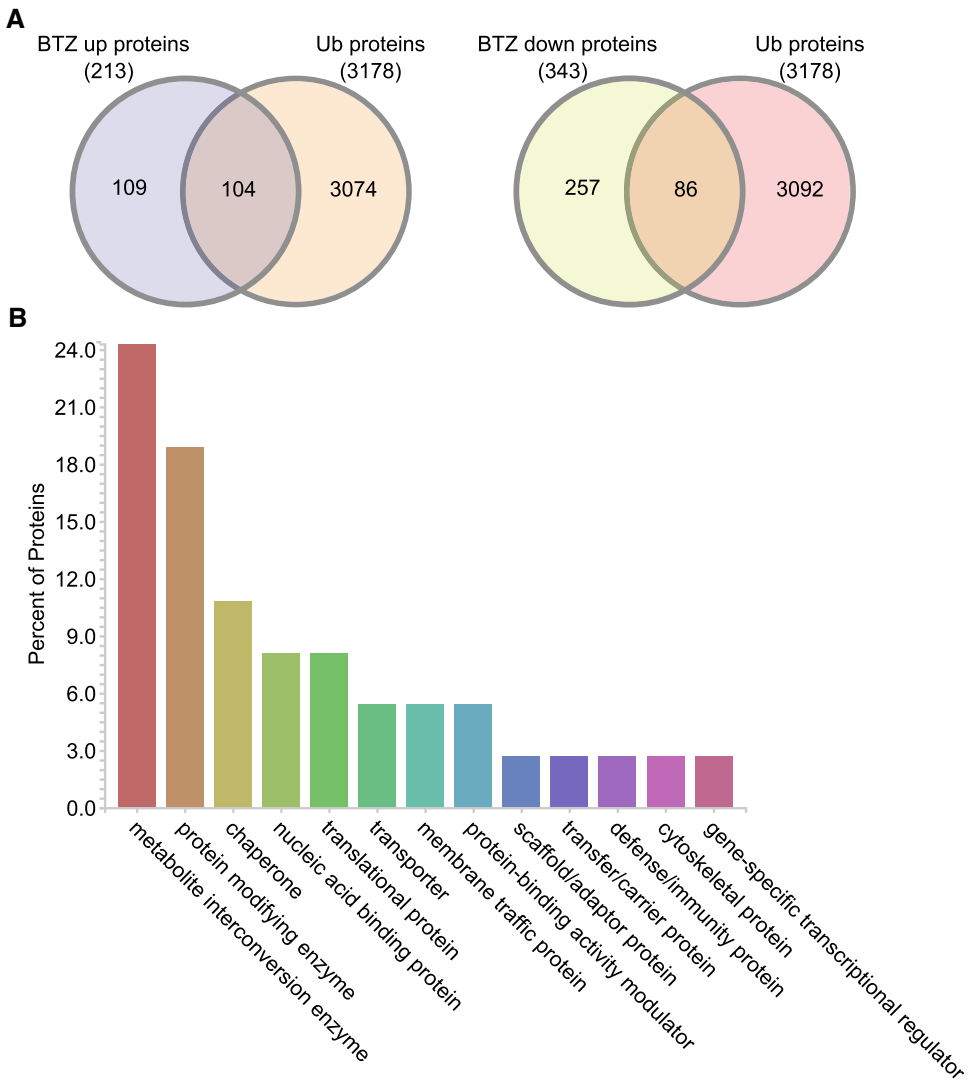

Figure 3. Identification of potential UPS substrates. **A)** Overlap between proteins that change in abundance following BTZ treatment with proteins that are diGly modified. **B)** PANTHER protein class annotations for the 104 proteins that increase in abundance following BTZ treatment and are diGly modified.

detected as being ubiquitinated in the root (Fig. 3A). Irrespective of changes in cognate protein abundance, we found that 433 diGly sites decrease following BTZ treatment (Supplementary Table S1). These proteins that were observed to be ubiquitinated but decreased upon BTZ treatment could be degraded by lysosomal proteolysis, via either lysosomes or autophagy pathways. Alternatively, these proteins could be degraded by specific proteases in a selective manner. These degradation processes have been shown to increase following 26S proteosome inhibition (Pandey et al. 2007; Laussmann et al. 2011; Marshall et al. 2015).

Motif analysis of ubiquitinated peptides identifies an enriched QK motif

Detailed biochemical studies of ubiquitination domains associated with protein degradation (termed "degrons") and bioinformatic motif analyses have identified a number of conserved amino acid motifs associated with ubiquitination (Varshavsky 1991; Dreher et al. 2006; Kim et al. 2011; Winkler et al. 2017). Using our catalog of localized diGly sites, we performed a motif analysis with motifeR to identify novel enriched motif(s) associated with ubiquitination within a 14 amino acid window. Among the full catalog of ubiquitinated sites (Supplementary Table S2), 27 significantly enriched motifs were detected. Notably, D, E, A, and G residues were the most prevalent amino acids surrounding the ubiquitinated lysine (Supplementary Fig. S3 and Table S7). A previous analysis from rice identified several enriched motifs among ubiquitinated peptides, including the EK^{ub} and GK^{Ub} motifs (Chen et al. 2018).

Next, we focused on the root samples to examine if there were any motifs present in surrounding the BTZ stabilized sites but not in the control samples (Supplementary Table S1). Among the diGly sites that were not increased following BTZ, we found an EK^{Ub} motif, as well as several other motifs lacking any comprehensive properties (Supplementary Fig. S4). We then examined the 1,336 diGly sites that increase in response to BTZ and uncovered a previously unreported QK^{Ub} motif, which was not enriched in the minus BTZ control samples (Fig. 4A). GO enrichment analyses of QK^{Ub} motif containing proteins determined that these proteins are involved in responses to plant growth regulators (auxin and karrikin), gene expression, and other biological processes (Fig. 4B and Supplementary Table S8). Additionally, proteins,

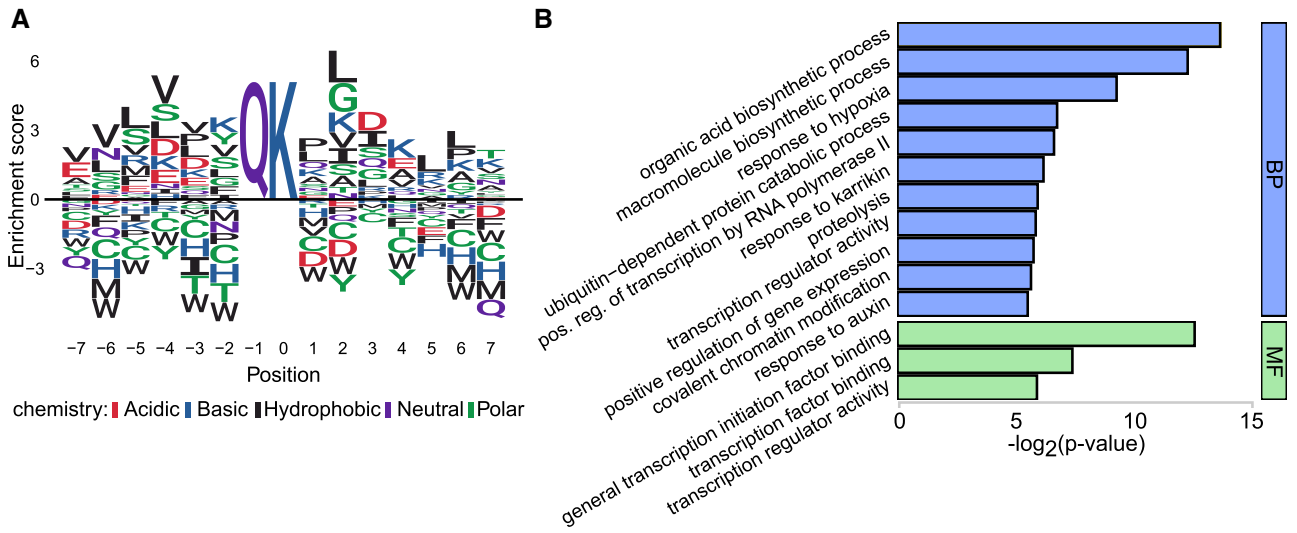

Figure 4. Ubiquitin motif analysis of BTZ increased diGly sites. **A)** Analysis of the 14 amino acid window surrounding the 1,336 diGly sites induced by BTZ identified an enriched QK^{Ub} motif. **B)** GO enrichment analyses of QK^{Ub} motif containing proteins. Supplementary Table S7 contains the full list of all identified enriched motifs surrounding ubiquitinated lysine residues.

which have the QK^{Ub} motif, are significantly enriched for TF molecular functions (Fig. 4B).

Ubiquitination of TFs is prevalent in roots and impacts protein stability

TFs were prominent among the classes of proteins detected as being ubiquitinated (Supplementary Table S2). A closer look at the modified TFs reveals that we identified 40 different TF families with ubiquitinated proteins (Fig. 5A). A number of these families contain many TFs that are ubiquitinated, for example the AP2-EREBP, AuxIAA, bHLH, homeobox, and NAC families each contain >40 ubiquitination sites. Notably, many of these TFs have been well established as UPS substrates, but the site(s) of ubiquitinated have not been previously identified (Kelley and Estelle 2012; Kelley 2018). Of particular interest are previously unreported ubiquitination sites on twelve Auxin/Indole-3-Acetic Acid (Aux/IAA) proteins (INDOLE-3-ACETIC ACID INDUCIBLE: IAA2–4, IAA7–9, IAA13, IAA16, IAA17, IAA26–28), four AUXIN RESPONSE FACTOR (ARFs) (ARF1, ARF2, ARF5, ARF7), six JASMONATE-ZIM-DOMAIN PROTEIN (JAZ) proteins (JAZ2–4, JAZ6, JAZ11, JAZ12), and three sites on ETHYLENE INSENSTIVE 3 (EIN3) (Fig. 5A and Supplementary Table S2). These findings pinpoint in vivo sites of ubiquitination for many well-studied TFs involved in hormone signaling and will certainly facilitate future biochemical studies on these TFs.

Given the key roles many TFs play in driving growth, development, and environmental responses we examined the functional consequence of their ubiquitination. We selected several TFs that had a single identified ubiquitination site and were available as full-length clones from the Arabidopsis Biological Resource Center (ABRC). We reasoned that the observed ubiquitination of these TFs may be linked to protein stability. In order to test this idea, we performed mutagenesis analyses and monitored protein stability using established luciferase based degradation assays (Gilkerson et al. 2016). For mutagenesis assays, lysine residues are typically mutated to arginine (so called K-to-R mutants) to block ubiquitination at that particular amino acid residue (Gilkerson et al. 2015). Using this approach, WT and K > R mutated TFs were expressed as LUCIFERASE (LUC) fusions in *Nicotiana benthamiana* and measured for protein abundance over time following cycloheximide (CHX) treatment. Three of the TFs we tested displayed an increase in the K > R mutated protein compared to the WT version of the TF level in these assays (Fig. 5B to D). This includes K166 on CRYPTOCHROME-INTERACTING BASIC-HELIX-LOOP-HELIX 1 (CIB1; AT4G34530), K180 on CIB1 LIKE PROTEIN 2 (CIL2; AT3G23690), and K271 on SENSITIVE TO PROTON RHIZOTOXICITY 1 (STOP1; AT1G34370). These results support the hypothesis that these lysine residues are required for ubiquitin mediated protein turnover.

Blocking ubiquitination of K166 on CIB1 promotes early flowering in short day conditions

CIB1 is a bHLH family TF, which physically interacts with CRYPTOCHROME 2 (CRY2) to positively regulate *FLOWERING LOCUS T* (*FT*) and promote flowering, in Arabidopsis (Liu et al. 2008). A previous study reported that CIB1 protein could be degraded by 26S proteasome, but the amino acid site(s) of ubiquitination were not known (Liu et al. 2013). In this study, we detected K166 as an ubiquitin site on CIB1 in root, seedling, and leaf tissues (Supplementary Table S2). Given that mutating K166 to R influences the stability of CIB1 in *N. benthamiana* (Fig. 5B), we decided to study this further using an in planta approach. For this, we employed CRISPR/Cas9 adenosine base editing of the endogenous *CIB1* locus to convert K166 to R166. Base editing has been used to create PTM nulls in mammalian systems and has been proposed in plants (Kong et al. 2021; Pramanik et al. 2021; Sankar et al. 2022). This approach has the potential to streamline functional characterization, eliminate transgene position effects, and minimize the need to extensively screen numerous transgenic lines to identify those with similar expression levels. We generated a base edited *CIB1* K166 > R allele using a modified rice ABE8e (rABE8e), which was previously been shown to be a high-efficiency adenine base editor (Wei et al. 2021). To mutate lysine 166 to arginine in *CIB1*, we designed a guide RNA to change the corresponding codon AAA to AGA or AGG at positions 675 and/or 676 base pairs in the *CIB1* gene. Wild-type Col-0 was transformed with the AtABE8e-NG-cib1 construct containing the adenine base editor and corresponding *CIB1* guide RNAs.

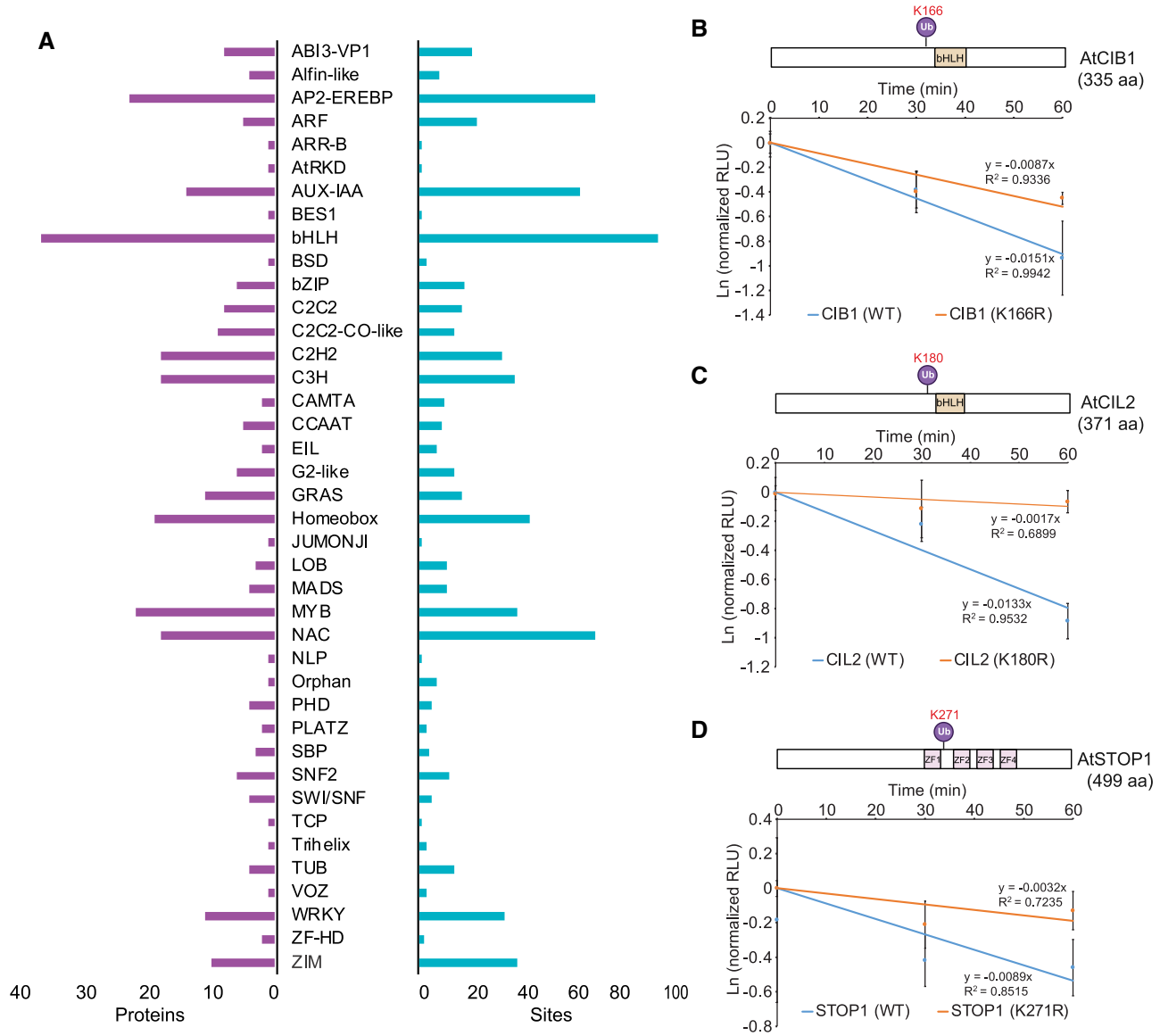

Figure 5. Analysis of TF ubiquitination. **A)** Number of ubiquitinated proteins (Left) and sites (Right) per TF family. **B)** to **D)** Testing the role of UBQ attachment on protein stability in vivo. Degradation assays on wild-type and K > R mutated proteins. Data are means of 3 independent replicates ± standard error for normalized RLU based on luciferase activity.

Sequence analysis of T2 plants indicated that the targeted codon was base edited from AAA (K) to AGG (R) (Fig. 6A) at a 3.6% frequency (1/28 independent T2 lines). We designated this base edited line *cib1-3*.

A previous study reported that *CIB1* overexpression lines exhibited early flowering (Liu et al. 2008). Thus, we measured the flowering time of WT and *cib1-3* grown under long day (16 h day, 8 h night) and short day (8 h day, 16 h night) conditions. Under long day conditions, both WT and *cib1-3* flowered at ~25 days (Supplementary Fig. S5A). Previously, it was shown that overexpression of *CIB1* results in early flowering under long day conditions (Liu et al. 2008). This discrepancy in observed flowering time may be due to overexpression of *CIB1* compared to expressing a stabilized form of *CIB1* from the endogenous promoter. However, under short day conditions *cib1-3* flowered significantly earlier than WT (Fig. 6B and C). To further explain the early flowering phenotype of *cib1-3*, we tested the expression level of *FT* in WT and *cib1-3* leaves. Consistent with the early flowering phenotype, *FT* expression levels were significantly higher in *cib1-3* than WT ($P < 0.05$) under short day conditions (Fig. 6D). In addition, the levels of *CIB1* mRNA were not changed in *cib1-3* compared to WT (Fig. 6E). These results suggest that the K116R mutation in *cib1-3* leads to increased protein levels of CIB1, but not mRNA, which in turn activates *FT* mRNA and leads to flowering. In contrast, the expression levels of both *FT* and *CIB1* were normal in WT and *cib1-3* under long day conditions (Supplementary Fig. S5B and C). These results demonstrate that the ubiquitin-mediated regulation of CIB1 at K166 may play a role in flowering time.

Final conclusions and outlook

This quantitative proteomics study provides a streamlined IP-MS/MS workflow for the identification of ubiquitination sites on plant proteins and a wealth of biochemical data for future functional follow-up assays. For example, the functional roles of the identified ubiquitination events using mutagenized proteins in planta can be tested using transgenic or CRISPR/Cas9-mediated base editing approaches. Additionally, it will be of great interest to

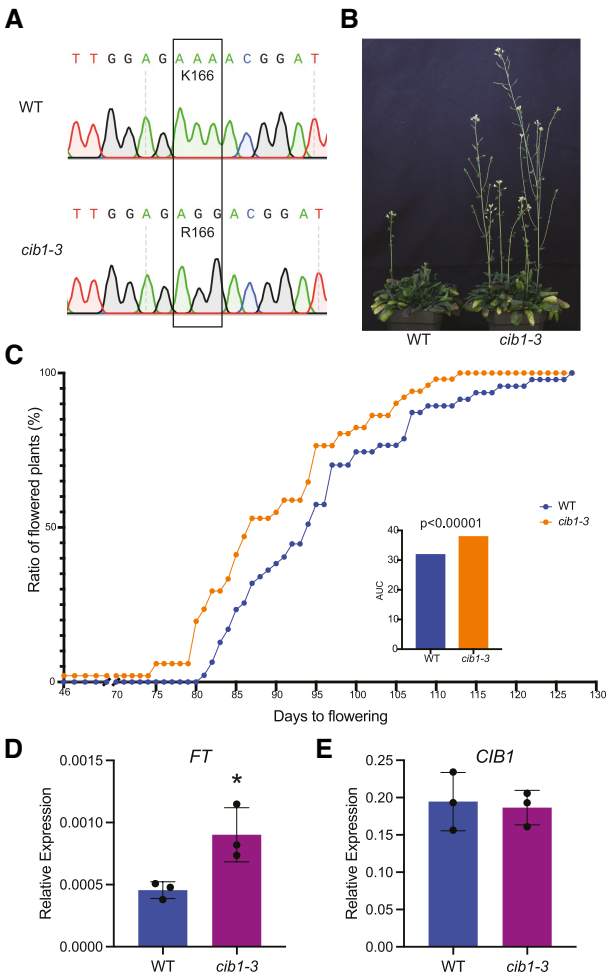

Figure 6. Blocking ubiquitination of CIB1 K166 promotes flowering. **A)** Sanger sequencing chromatograms of WT and *cib1-3*. **B)** 96-day old WT and *cib1-3* plants grown under SD conditions. **C)** Time to flowering of WT ($n = 47$) and *cib1-3* ($n = 51$). Inset shows the area under curve (AUC) of flowering time. **D** and **E)** Relative expression level of *FT* and *CIB1* in WT and *cib1-3* (*, $P < 0.05$) (DeLong et al. 1988). Data represent means ± SD from 3 independent biological replicates where each replicate is a single plant.

identify the substrate-E3 ligase interactions underlying these modifications as many E3 ubiquitin ligases in Arabidopsis are still without known substrates (Vierstra 2012; Kelley 2018; Lee et al. 2018). As future quantitative catalogs are expanded across tissues and environmental responses, we can begin to examine spatial and context-specific events that are associated with ubiquitination in planta.

Materials and methods

Growth and treatment conditions of Arabidopsis roots

Arabidopsis (*A. thaliana*) Col-0 seeds were surfaced sterilized in 50% bleach with 0.1% Tween-20 for 10 min and rinsed five times with sterile water before plating on 0.5× Murashige and Skoog (MS) media supplemented with 1% sucrose and 0.8% agarose overlaid with presterilized 110-μm nylon mesh. Col-0 seedlings were grown for 10 days in a growth chamber under 150 μmol m^{-2} s^{-1} long-day conditions (16 h light, 8 h dark) at 23 °C. Ten-day-old Col-0 seedlings were treated with either mock solution (equal volume of DMSO solvent control) or 100 μM BTZ for 3 h. Following treatments, ~3 g of pooled root or whole seedling tissue was harvested per replicate, immediately frozen into liquid nitrogen, and stored at −80 C. Three independent biological replicates were used per treatment.

Rosette leaves from 3-week-old Arabidopsis Col-0 grown under long day conditions at 23 °C were excised from the plant and overlaid on 100 μM BTZ dissolved in 0.5× MS for 2 h in petri dishes. After the BTZ treatment, the leaf tissue was quickly blotted on Kimwipes to remove excess solution and snap frozen in liquid nitrogen. Leaf tissue was stored at −80 °C prior to protein extraction.

Protein extraction and proteomics analyses

Protein extraction and digestion were done using the Phenol-FASP method (Song et al. 2018, 2020). For this, Arabidopsis root tissue was ground for 15 min under liquid nitrogen using a mortar and pestle. Next, 5 volumes of Tris buffered phenol pH 8 (buffer:tissue, v:w) was added to each sample tube, which was vortexed for 1 min. The samples were then vortexed for 1 more minute with 5 volumes (buffer:tissue, v:w) of extraction buffer (50 mM Tris pH 7.5, 1 mM EDTA pH 8, 0.9 M sucrose, 1× phosphatase inhibitors, 10 mM N-ethylmaleimide, and then centrifuged at 13,000×g for 10 min at 4 °C. The phenol phase was transferred to a new tube and a second phenol extraction was performed on the aqueous phase. The two phenol phase extractions were combined and 5 volumes of prechilled methanol with 0.1 M ammonium acetate was added and mixed well, then kept at −80 °C for 1 h prior to centrifugation at 4,500×g for 10 min at 4 °C. Precipitation with 0.1 M ammonium acetate in methanol was performed twice with incubation at −20 °C for 30 min. The sample was resuspended in 70% methanol and kept at −20 °C for 30 min prior to centrifuging at 4,500×g, for 10 min at 4 °C. The supernatant was discarded, and the pellet was placed in a vacuum concentrator till near dry. Two volumes (buffer:pellet, v:v) of protein extraction buffer (8 M urea, 50 mM Tris pH 7, 5 mM tris(2-carboxyethyl)phosphine (TCEP), 1× phosphatase inhibitors, and 10 mM N-ethylmaleimide) was added to the pellet. The samples were then probe sonicated to aid in resuspension of the pellet. The protein concentration was then determined using the Bradford assay (Thermo Scientific).

Filter aided sample preparation

The solubilized protein (~2.5 mg in 0.5 mL) was mixed with 3.5 mL urea solution (8 M urea, 100 mM Tris pH 8, 1× phosphatase inhibitors, and 10 mM N-ethylmaleimide), added to an Amicon Ultracel–30 K centrifugal filter, and centrifuged at 4,000×g for 40–60 min. This step was repeated once. Then, 4 mL of urea solution with 2 mM TCEP was added to the filter unit and centrifuged at 4,000×g for 20–40 min. Next, 2 mL IAM solution (50 mM IAM in urea solution) was added and incubated without mixing at room temperature for 30 min in the dark prior to centrifuging at 4,000×g for 20–40 min. Two mL of urea solution was added to the filter unit, which was then centrifuged at 4,000×g for 20–40 min. This step was repeated once. Two milliliter of 0.05 M NH_4HCO_3 with 1× phosphatase inhibitors and 10 mM N-Ethylmaleimide was added to the filter unit and centrifuged at 4,000×g for 20–40 min. This step was repeated once. Then, 2 mL of 0.05 M NH_4HCO_3 solution with trypsin (enzyme to protein ratio 1:100) was added. Samples were incubated at 37 °C overnight. Undigested protein was estimated using Bradford assays, then trypsin (1 μg/μL) was added to a ratio of 1:100 and an equal volume of Lys-C (0.1 μg/μL) were added to the sample and incubated for an additional 4 h at 37 °C. The filter unit was added to a new collection tube and centrifuged at 4,000×g for 20–40 min. One milliliter of

0.05 M NH_4HCO_3 was added and centrifuged at 4,000×g for 20–40 min. The samples were acidified to pH 2–3 with 100% formic acid and centrifuged at 21,000×g for 20 min. Finally, samples were desalted using 100 mg or 500 mg Sep-Pak C18 cartridges (Waters). Eluted peptides were dried using a vacuum centrifuge (Thermo) and resuspended in 0.1% formic acid. Peptide amount was quantified using the Pierce BCA Protein assay kit.

Di-glycine lysine peptide enrichment

Peptides containing a diGly lysine remnant were enriched using anti-diGly lysine antibody conjugated agarose beads (PTM BIO, Cat# PTM-1104). In each experiment below, anti-diGly lysine antibody conjugated agarose beads were prewashed 3 times using 0.5 mL ice-cold phosphate buffered saline (PBS). Then, C18 desalted peptides (see amount below) resuspended to a final concentration of 5 mg/mL in IP/Wash buffer were combined with PBS prewashed anti-diGly lysine antibody-conjugated agarose beads (see below for amount) and rotated overnight at 4 °C. The next day, the sample was centrifuged at 500 g for 1 min and the supernatant was removed. The beads were then washed 3 times by adding 0.5 mL IP/Wash buffer (100 mM NaCl, 1 mM EDTA, 20 mM Tris-HCl, pH8), mixed by inverting for 30 s, and then centrifuging at 500×g for 1 min. After the last wash step, 0.5 mL of 0.1% trifluoroacetic acid (TFA) was added, which was followed by 1 min gentle rotation at room temperature to elute the bound peptides. The eluted peptides were collected by centrifugation at 1,000×g for 1 min at room temperature, and then transferred to a new tube. The elution steps were repeated two more times. Note that for the last elution step, the beads were rotated in 0.1% TFA for 5 min instead 1 min. The eluted peptides from each step were combined together, vacuum centrifuged to dry, and stored at −80 °C

For the root "2D-label free" experiment (Fig. 1D and E), 20 mg C18 desalted peptides and 1.6 mg anti-diGly lysine antibody conjugated agarose beads (PTM BIO, Cat# PTM-1104, Lot# TAIA29B01) were used. Specifically, the 20 mg peptides were resuspended with 3.6 mL IP/Wash buffer and then 600 µL of the resuspended peptides were aliquoted to individual 1.5 mL tubes. Next, 66.6 µL of PBS prewashed anti-diGly lysine antibody conjugated agarose beads were added to each tube and rotated overnight at 4 °C. The beads were washed, and peptides eluted as described above. Eluted peptides were stored at −80 °C.

For the root "Enrich -> TMT" experiments (Fig. 1D and E), 2 mg of C18 desalted peptides per IP were resuspended with 400 µL IP/Wash buffer, combined with 0.16 mg of PBS prewashed anti-diGly lysine antibody conjugated agarose beads (PTM BIO, Cat# PTM-1104, Lot# TAIA29B01) and, rotated overnight at 4 °C. The beads were washed, and peptides eluted as described above. Eluted peptides were stored at −80 °C until TMT labeling.

For the root "TMT -> Enrich" test (Fig. 1D), 18 mg of pooled TMT labeled peptides were desalted using 500 mg Sep-Pak C18 cartridges (waters) and enriched using 1.2 mg of anti-diGly lysine antibody (PTM BIO, Cat# PTM-1104, Lot# TAIA29B01) as described above.

The antibody-input peptides ratio tests experiment with seedling tissue were performed with 0.16 mg anti-diGly lysine antibody (PTM BIO, Cat# PTM-1104, and Lot# TAM0214B01) and the different amount of peptides list in Fig. 1B and C. One third of the enriched peptides from each sample were analyzed by 1D-LC-MS/MS for the ratio test. The remaining two thirds of the peptides from each enrichment were pooled and analyzed by 2D-LC-MS/MS. For the 3-week-old rosette leaf tissue ubiquitinome 0.8 mg anti-diGly lysine antibody (PTM BIO, Cat# PTM-1104, Lot# TAM0214B01) was used to enriched from 20 mg peptides.

TMT labeling

TMT10plex label reagents (ThermoFisher, Lot #TC264166) and TMTpro 16plex (ThermoFisher, Lot #UH290430) label reagents were used to label the anti diGly lysine antibody enriched peptides according to a modified labeling method (Song et al. 2020). The diGly enriched samples were labeled as follows. All peptides that were recovered following diGly enrichment, from each sample, were resuspended with 20 µL of 0.2 M HEPES buffer pH 8.5 (Alfa Aesar Cat# J63218) and then mixed with 0.08 mg TMT or TMTpro reagent that was resuspended in 8 µL dry acetonitrile (Millipore cat# AX0143-7). After 2-h incubation at room temperature, 1.6 µL of 5% hydroxylamine were added to each tube and vortexed. The samples were incubated at room temperature for 15 min to quench the labeling reaction. Next, the 9 samples were mixed together and stored at −80 °C.

For the TMTpro protein abundance runs, 10 µg of C18 desalted peptides were resuspended in 20 µL of 0.2 M HEPES buffer pH 8.5 and then mixed with 0.08 mg TMT reagent that was resuspended in 8 µL dry acetonitrile. After 2-h incubation at room temperature, 1.6 µL of 5% hydroxylamine were added to each tube and vortexed. The samples were incubated at room temperature for 15 min to quench the labeling reaction. Next, the samples were mixed together and stored at −80 °C.

LC/MS-MS of root samples

An Agilent 1,260 quaternary HPLC was used to deliver a flow rate of ~300 or 600 nL per minute for 100 or 200 internal diameter (ID) packed nanospray emitter tips respectively, via a splitter. All columns were packed in house using a Next Advance pressure cell and the nanospray tips were fabricated using fused silica capillary that was pulled to a sharp tip using a laser puller (Sutter P-2000).

2D-label free LC-MS/MS of root peptides

All of the diGly enriched peptides were loaded onto 10 cm capillary columns packed with 5 µM Zorbax SB-C18 (Agilent), which was connected using a zero dead volume 1 µm filter (Upchurch, M548) to a 5 cm long strong cation exchange (SCX) column packed with 5 µm polysulfoethyl (PolyLC). The SCX column was then connected to a 20 cm long nanospray tip (100 µm ID) packed with 2.5 µM C18 (Waters). The 3 sections were joined and mounted on a custom electrospray source for on-line nested peptide elution. Peptides were eluted from the loading column unto the SCX column using a 0% to 80% acetonitrile gradient over 60 min. Peptides were then fractionated from the SCX column using a series of salt steps. The following ammonium acetate salt steps were used: 25, 45, 60, 70, 80, 90, 100, 300, 500, and 1000 mM. For these analyses, buffers A (99.9% H_2O, 0.1% formic acid), B (99.9% ACN, 0.1% formic acid), C (100 mM ammonium acetate, 2% formic acid), and D (1 M ammonium acetate, 2% formic acid) were utilized. For each salt step, a 150-minute gradient program comprised of a 0 to 5 min increase to the specified ammonium acetate concentration, 5 to 10 min hold, 10 to 14 min at 100% buffer A, 15 to 100 min 5% to 30% buffer B, 100–121 min 30% to 45% buffer B, 120 to 140 min 45% to 80% buffer B, 140 to 144 min 80% buffer B, and 145 to 150 min buffer A was employed.

Eluted peptides were analyzed using a Thermo Scientific Q-Exactive Plus high-resolution quadrupole Orbitrap mass spectrometer, which was directly coupled to the HPLC. DDA was obtained using Xcalibur 4.0 software in positive ion mode with a spray voltage of 2.00 kV and a capillary temperature of 275 °C and an RF of 60. MS1 spectra were measured at a resolution of 70,000, an automatic gain control (AGC) of 3e6 with a maximum

ion time of 100 ms and a mass range of 400–2000 m/z. Up to 15 mS2 were triggered at a resolution of 17,500 with a fixed first mass of 120 m/z. An AGC of 1e5 with a maximum ion time of 50 ms, an isolation window of 1.3 m/z, and normalized collision energy of 28 were used for this run. Charge exclusion was set to unassigned, 1, 5 to 8, and >8. MS1 that triggered MS2 scans were dynamically excluded for 25 s.

"Enrich -> TMT" 2d-TMT LC-MS/MS of root peptides

All of the TMT labeled diGly lysine enriched peptides were loaded onto 10 cm capillary columns packed with 5 μM Zorbax SB-C18 (Agilent), which was connected using a zero dead volume 1 μm filter (Upchurch, M548) to a 5 cm long SCX column packed with 5 μm PolySulfoethyl (PolyLC). The SCX column was then connected to a 20 cm nanospray tip (200 μm ID) packed with 2.5 μM C18 (Waters). The 3 sections were joined and mounted on a custom electrospray source for on-line nested peptide elution. Peptides were eluted from the loading column unto the SCX column using a 0% to 80% acetonitrile gradient over 60 min. Peptides were then fractionated from the SCX column using these ammonium acetate salt steps: 35, 70, 100 and 1000 mM.

Eluted peptides were analyzed using a Thermo Scientific Q-Exactive Plus high-resolution quadrupole Orbitrap mass spectrometer, which was directly coupled to the HPLC. DDA was obtained using Xcalibur 4.0 software in positive ion mode with a spray voltage of 2.00 kV and a capillary temperature of 275 °C and an RF of 60. MS1 spectra were measured at a resolution of 70,000, an AGC of 3e6 with a maximum ion time of 100 ms and a mass range of 400–2000 m/z. Up to 15 mS2 were triggered at a resolution of 35,000 with a fixed first mass of 120 m/z. An AGC of 1e5 with a maximum ion time of 50 ms, an isolation window of 1.3 m/z, and a normalized collision energy of 33 were used for this analysis. Charge exclusion was set to unassigned, 1, 5 to 8, and >8. MS1 that triggered MS2 scans were dynamically excluded for 25 s.

"Enrich -> TMTpro" 2d-TMTpro LC-MS/MS of root peptides

All of the TMTpro labeled diglycine lysine enriched peptides were loaded onto 10 cm capillary columns packed with 5 μM Zorbax SB-C18 (Agilent), which was connected using a zero dead volume 1 μm filter (Upchurch, M548) to a 5 cm long SCX column packed with 5 μm polysulfoethyl (PolyLC). The SCX column was then connected to a 20 cm nanospray tip (100 μm ID) packed with 2.5 μM C18 (Waters). The 3 sections were joined and mounted on a custom electrospray source for on-line nested peptide elution. Peptides were eluted from the loading column unto the SCX column using a 0% to 80% acetonitrile gradient over 60 min. Peptides were then fractionated from the SCX column using a series of salt steps. The following ammonium acetate salt steps were used: 30, 60, 80, 90, 95, 100, 200, and 1000 mM. Eluted peptides were analyzed using a Thermo Scientific Q-Exactive Plus high-resolution quadrupole Orbitrap mass spectrometer using acquisition settings described in "*Enrich -> TMT" 2D-TMT LC-MS/MS*" except a normalized collision energy of 31 were used for this analysis.

TMTpro protein abundance analysis of root peptides

Ten μg of the pooled TMTpro labeled peptides were loaded onto 10 cm capillary column packed with 5 μM Zorbax SB-C18 (Agilent), which was connected using a zero dead volume 1 μm filter (Upchurch, M548) to a 5 cm long SCX column packed with 5 μm polysulfoethyl (PolyLC). The SCX column was then connected to a 20 cm nanospray tip (100 μm ID) packed with 2.5 μM C18 (Waters). The 3 sections were joined and mounted on a custom electrospray source for on-line nested peptide elution. Peptides were eluted from the loading column unto the SCX column using a 0% to 80% acetonitrile gradient over 60 min. Peptides were then fractionated from the SCX column using a series of salt steps. The following ammonium acetate salt steps were used: 30, 60, 70, 75, 80, 82.5, 85, 87.5, 90, 92.5, 95, 97.5, 100, 125, 150, 200, and 1000 mM.

Eluted peptides were analyzed using a Thermo Scientific Q-Exactive Plus high-resolution quadrupole Orbitrap mass spectrometer, which was directly coupled to the HPLC. DDA was obtained using Xcalibur 4.0 software in positive ion mode with a spray voltage of 2.2 kV and a capillary temperature of 275 °C and an RF of 60. MS1 spectra were measured at a resolution of 70,000, an AGC of 3e6 with a maximum ion time of 100 ms and a mass range of 400–2000 m/z. Up to 15 mS2 were triggered at a resolution of 17,500 or 35,000 was used for two replicate runs respectively. Note that the TMTpro labels used here have 1 Da spacing between reporter ion, which enables acquisition with the 17,500 resolution setting. A fixed first mass of 120 m/z. An AGC of 1e5 with a maximum ion time of 50 ms, an isolation window of 1.3 m/z, and a normalized collision energy of 31 were used. Charge exclusion was set to unassigned, 1, 5 to 8, and >8. MS1 that triggered MS2 scans were dynamically excluded for 25 s.

LC/MS-MS of seedling and leaf samples

Off-line basic-reversed phase fractionation for 2D fractionation experiments were performed using a Thermo Scientific UltiMate 3000 UHPLC setup for loss-less nano-fractionion based on an approach described by Kulak et al. (2017). Peptides were loaded on a CoAnn Technologies HpH column that is 25 cm long, with a 200 μm ID, and packed with 3 μm C18 (300A). Peptides were separated at a flow-rate of 1.25 μL min^{-1} for 120 min using 10 mM ammonium hydroxide in optima H_2O as solution A and 80% acetonitrile in 10 mM ammonium hydroxide as solution B, and the following gradient: from 6% to 37% B in 60 min, from 37% to 56% B in 20 min, and a final wash at 99% B through the next 5 min. Fractions were collected every 60 s and concatenated into eight fractions. Each fraction was subsequently analyzed as follows

A Thermo Vanquish Neo UHPLC was used to deliver peptides to Thermo Scientific Orbitrap Exploris 480 mass spectrometer. The Vanquish Neo was operated in "heated trap-and-elute, backward flush" mode. Peptides were desalted and concentrated on a PepMap Neo trap column (300 μM i.d.×5 mm, 5 μm C18, 100 Å μ-Precolumn, Thermo Scientific) at a flow rate of 10 μL min^{-1}. Peptide separation was performed on a 110 cm micro-pillar array column (μ-PAC Neo, Thermo Scientific) with a flow rate of ~300 nL min^{-1} over a 120 min reverse phase active gradient (80% ACN in 0.1% FA from 8% to 28% over 112 min, from 28% to 48% in 8 min) followed by a column/trap wash at 80% ACN for 10 min. Eluted peptides were analyzed using a Thermo Scientific Orbitrap Exploris 480 mass spectrometer, directly coupled to the UHPLC through an Easy Spray Ion source (Thermo Scientific). DDA was obtained using Xcalibur 4.0 software in positive ion mode with a spray voltage of 1.9 kV, a capillary temperature of 280 °C. MS1 spectra were measured at a resolution of 120,000, an AGC of 3e6 with auto maximum ion time, and a mass range of 375–1450 m/z. Top 40 mS2 were captured at a resolution of 15,000. A fixed first mass of 120 m/z. An AGC of 5e4 with maximum ion time set to automatic, normalized collision energy of 29, and an isolation window of 2 m/z were used. Charge inclusion was set to 2–5. MS1 that triggered MS2 scans were dynamically excluded for 30 s. Additionally, a m/z and z exclusion table during

RT 60 to 80 min was used to filter specific peptides on "precursors exclusion" experiments (Supplementary Fig. S1).

Database search and FDR filtering

All of the raw data were analyzed together using MaxQuant version 1.6.7.0. Spectra were searched against Arabidopsis TAIR10 genome, which was complemented with reverse decoy sequences and common contaminants by MaxQuant. Carbamidomethyl cysteine was set as a fixed modification while methionine oxidation and protein N-terminal acetylation were set as variable modifications. In experiments where we searched for diGly sites "GlyGly(K)" was set as a variable modification. Digestion parameters were set to "specific" and "Trypsin/P;LysC." For the TMT experiments, the sample type was set to "Reporter Ion MS2" with "10plex TMT" or "TMTpro16plex" selected for both lysine and N-termini. Up to two missed cleavages were allowed. A false discovery rate <0.01 at both the peptide spectral match and protein identification level was required. The "second peptide" option was used to identify co-fragmented peptides. The "match between runs" feature of MaxQuant was not utilized. We retained tryptic K-ε-GG cleavage sites as trypsin cleaves these sites, which are effectively enriched using anti-diGly lysine antibodies (Sun et al. 2023).

Statistical analyses of proteomics data

Statistical analyses on the protein abundance and ubiquitination data were performed using TMT-NEAT Analysis Pipeline version 1.3 (https://github.com/nmclark2/TMT-Analysis-Pipeline) (Clark et al. 2021). First, the MaxQuant output table was trimmed to only include the columns needed for statistical analysis and the columns were re-labeled using the provided sample information. Contaminants and reverse hits were removed at this stage. Prior to normalization, the two technical replicates for the abundance run were combined. Next, data were normalized using the sample loading normalization method (Plubell et al. 2017). Finally, statistical analysis was performed on the normalized values using PoissonSeq (Li et al. 2012). All resulting *P*- and *q*-values are retained and reported in Supplementary Tables S1 and S3 so that readers can use their preferred cutoff for selecting proteins and PTM sites that change after treatment for follow up studies. For our analyses, we classified protein groups (FC >1.1 and *P*-value <0.05) and PTMs (FC >1.1 and *q*-value <0.1) as differentially accumulating.

Functional annotations and enrichment

GO overrepresentation tests were performed using PANTHER (Mi et al. 2019) with all proteins containing a diGly site as the input and all *A. thaliana* genes in the database as the reference (Fig. 1D). The test type selected was "Fisher" with FDR correction. GO terms with a FDR < 0.05 are considered enriched. Potential UPS substrates were categorized using PANTHER protein class annotations (Fig. 2B). TFs were annotated based obtained from (Yilmaz et al. 2009) and (Pruneda-Paz et al. 2014).

Motif analyses

Motif enrichment was performed in R using the motifeR package (Wang et al. 2019a). We used default settings including a 14 amino acid window size, 20 as the minimum number of sites, and a *P*-value of 0.000001 for the analysis. Lysine was set as the central residue and the TAIR10 proteome was used as the background reference. Sequence logo was constructed using Logolas R package and plotted using ggseqlogo R package (Wagih 2017; Dey et al. 2018). Analyses were performed in R version 3.6.2. GO enrichment analysis was performed using ClueGO app v2.5.7 on Cytoscape v3.8.0 (Shannon et al. 2003; Bindea et al. 2009).

Reverse transcription quantitative PCR

Homozygous *cib1-3* T4 plants and WT control (segregated from the same *cib1-3* T2 heterozygote plant) grown in both long day (16 h light at 22 °C, 8 h dark at 20 °C) and short day (8 h lights at 22 °C, 16 h dark at 20 °C) conditions were used for RNA extraction. All above ground tissue (55 days old for short day or 20 days old for long day conditions) was collected at ZT4. Total RNA was extracted with Trizol (Invitrogen) and Direct-zol RNA MiniPrep kit (Zymo Research). cDNA was synthesized with LunaScript RT SuperMix Kit (NEB). Quantitative PCR was done with the following program: 3 min at 95 °C, followed by 39 cycles of 10 s at 95 °C, 10 s at 60 °C, and 30 s at 72 °C with a CFX96^{TM} Real-Time system (Bio-Rad). The ΔΔCt method was used to analyze the gene expression data. Primers are listed in Supplementary Table S9.

Plasmid construction and plant transformation

Full-length cDNA clones in pENTR/D-Topo were obtained from the ABRC for the following TFs: CIB1/AT4G34530 (TOPO-U14-E03), CIL2/AT3G23690 (TOPO-U07-C08), and STOP1/AT1G34370 (TOPO-U16-C08). Primers used are described in Supplementary Table S9. Lysine sites of interest were mutated to arginine (K > R) using the Q5 Site-Directed Mutagenesis Kit (New England Biolabs, E0554) as described by the manufacturer. Primers for site directed mutagenesis were designed with NEBaseChanger and are listed in Supplementary Table S9. Positive clones with the desired mutations were confirmed by restriction enzyme digest and Sanger sequencing. Both WT and K > R pENTR/D-Topo clones were subsequently cloned into a modified p35S-LUC destination vector named "pDO18" using LR Clonase (Thermo Fisher Scientific). pDO18 was generated by amplifying the Firefly luciferase coding sequence from pBGL7.0 and inserted into the SpeI restriction sites in the pCMS44 vector, which is derived from p2BGW7. pCMS44 was created by mutating p2BGW7 using the Q5 site-directed mutagenesis kit and primers Q5SDM_7/16/2018_F and Q5SDM_7/16/2018_R to contain XhoI and KpnI restriction sites between the attR2 and T35S sequences. The wild-type and mutated K > R TF clones in the pDO18 backbone were verified by restriction digest and transformed into Agrobacterium strain GV3101.

The plasmid (AtABE8e-NG) used for *cib1* base editing was constructed by two steps of Gibson assembly, first step, the fragment of ProAtU6-29 was cloned from Arabidopsis genome (Col-0) with forward primer SGY502 and reverse primer SGY503, then Gibson assembly with the fragment of rABE8e (NG) (Wei et al. 2021) backbone harvested from the enzyme digestion fragment with HindIII and BsaI to generate the intermediate plasmid pABE8eNG-AtU6-29, which replaced the OsU6 promoter with the promoter of AtU6-29. The second step, to replace the hygromycin resistance gene (HygR) with phosphinothricin acetyltransferase gene (Bar), the fragment of Bar was PCR amplified from plasmid pGWB602 with forward primer SGY506 and reverse primer SGY507, then Gibson assembly with the fragment of plasmid backbone amplified from pABE8eNG-AtU6-29 with forward primer SGY504 and reverse primer SGY505. gRNA primer SGY514 and SGY515 for *cib1* base editing was inserted into BsaI site of plasmid to generate AtABE8e-NG-cib1, which was transformed into Agrobacterium strain GV3101. The transgenic Arabidopsis for *cib1* base editing

were generated by floral dip with Arabidopsis Col-0 (Clough and Bent 1998).

N. benthamiana infiltration and CHX treatment

Agrobacterium containing construct of interest was grown overnight in YEB medium supplemented with appropriate antibiotics at 28 °C. Cell pellets were resuspended and then infiltrated into *N. benthamiana* leaves. Plants were grown under light for 48 h and leaf discs were obtained from the infiltrated region of the leaves. The leaf discs were incubated in liquid MS medium containing 1% sucrose in the presence of 200 μM CHX or DMSO (control) for 30 and 60 min. The start of the first measurement following CHX treatment was designated time 0. Pooled leaf discs (~ 60 mg) were blotted on a paper tower and flash frozen in liquid nitrogen, ground into powder and dissolved in 200 μL 1× cell culture lysis reagent (Promega), followed by centrifugation for 15 min at 4 °C. 10 μL of the clear supernatant was used for LUC detection. The LUC activities were measured with the Luciferase Assay System (Promega) on a microplate reader. The relative light units (RLU) for each sample were analyzed as previously described (Gilkerson et al. 2016).

Analysis of flowering time

Homozygous *cib1-3* T4 plants and WT control (segregated from the same *cib1-3* T2 heterozygote plant) grown in both long day (16 h light at 22 °C, 8 h dark at 20 °C) and short day (8 h lights at 22 °C, 16 h dark at 20 °C) conditions. The flowering time was recorded for each single plant by scoring for presence of floral meristem every day starting from 20 days after planting for long day conditions and 40 days after planting for short day conditions. Statistical differences in flowering time between *cib1-3* and WT were determined by comparing area under the curve (AUC). DeLong's test was performed to obtain Z-statistic score for AUC. Additionally, *P*-value of the Z-statistic score from AUC was obtained using (https://www.socscistatistics.com/pvalues/normaldistribution.aspx) (DeLong et al. 1988).

Accession numbers

Accession numbers are listed in Supplementary Tables S1, S2, and S9.

Author contributions

Conceptualization, funding acquisition, project administration, and supervision by J.W.W and D.R.K. Data curation by G.S. and N.M.C. Formal analysis by D.O., N.M.C., and C.M. Investigation and validation by G.S., D.O., S.M., and Y.P. Methodology by G.S., D.O., C.M., C.J., Y.P., D.R.K., and J.W.W. Software by N.M.C. Visualization and writing by J.W.W., D.R.K., G.S., D.O., and C.M.

Supplementary data

The following materials are available in the online version of this article.

Supplementary Figure S1. Exclusion test for LC-MS/MS runs with diGly peptides enriched samples.

Supplementary Figure S2. Summary of ubiquitinome coverage.

Supplementary Figure S3. Significantly enriched motifs from all detected diGly sites.

Supplementary Figure S4. Ubiquitin motif analysis.

Supplementary Figure S5. Blocking ubiquitination of CIB1 K166 does not alter days to flowering under long day conditions.

Supplementary Table S1. Root ubiquitinome.

Supplementary Table S2. All detected diGly sites.

Supplementary Table S3. Published ubiquitinome studies reporting at the ubiquitin site level in Arabidopsis.

Supplementary Table S4. Enriched GO Biological Process terms among all proteins with detected diGly modification.

Supplementary Table S5. Quantified changes in protein abundance following BTZ treatment of Arabidopsis roots.

Supplementary Table S6. Summary of spectra and diGly-modified lysine sites from nonenriched and diGly(K) enriched peptides.

Supplementary Table S7. Enriched motif of all detected diGly sites.

Supplementary Table S8. Enriched GO terms among the QK^{Ub} motif containing proteins.

Supplementary Table S9. Primers used in this study.

Supplementary Table S10. Summary of statistical assays.

Funding

This work was supported by the Iowa State University (ISU) Plant Science Institute, NIH (R01GM120316), NSF (IOS-1759023), DOE (DE-SC0023158), and USDA NIFA Hatch project IOW3808 funds to J.W.W.; USDA NIFA Hatch project IOW3649 and ISU startup funds to D.R.K.; ISU Crop Bioengineering Center Seed Grants to D.R.K and J.W.W.; and USDA NIFA Postdoctoral Research Fellowship (2019-67012-29712) to N.M.C.

Conflict of interest statement. None declared.

Data availability

The original MS proteomics raw data, as well as the MaxQuant output files, may be downloaded from MassIVE (http://massive.ucsd.edu) using the identifier: MSV000086156 (root), alkylation reagent tests (MSV000095495), and all diGly runs (MSV000095496). All other data are provided in the Supplementary Tables. A summary of statistical assays is provided in Supplementary Table S10. Plasmids and seed stocks are available upon request.

References

Abu Hatoum O, Gross-Mesilaty S, Breitschopf K, Hoffman A, Gonen H, Ciechanover A, Bengal E. Degradation of myogenic transcription factor MyoD by the ubiquitin pathway in vivo and in vitro: regulation by specific DNA binding. *Mol Cell Biol*. 1998:18(10):5670–5677. https://doi.org/10.1128/MCB.18.10.5670

Aguilar-Hernández V, Kim D-Y, Stankey RJ, Scalf M, Smith LM, Vierstra RD. Mass spectrometric analyses reveal a central role for ubiquitylation in remodeling the Arabidopsis proteome during photomorphogenesis. *Mol Plant*. 2017:10(6):846–865. https://doi.org/10.1016/j.molp.2017.04.008

Ahn MY, Oh TR, Seo DH, Kim JH, Cho NH, WT K. Arabidopsis group XIV ubiquitin-conjugating enzymes AtUBC32, AtUBC33, and AtUBC34 play negative roles in drought stress response. *J Plant Physiol*. 2018:230:73–79. https://doi.org/10.1016/j.jplph.2018.08.010

Berger N, Demolombe V, Hem S, Rofidal V, Steinmann L, Krouk G, Crabos A, Nacry P, Verdoucq L, Santoni V. Root membrane ubiquitinome under short-term osmotic stress. *Int J Mol Sci*. 2022:23(4):1956. https://doi.org/10.3390/ijms23041956

Bindea G, Mlecnik B, Hackl H, Charoentong P, Tosolini M, Kirilovsky A, Fridman WH, Pagès F, Trajanoski Z, Galon J. ClueGO: a cytoscape plug-in to decipher functionally grouped gene ontology

and pathway annotation networks. *Bioinformatics*. 2009:25(8):1091–1093. https://doi.org/10.1093/bioinformatics/btp101

Cadwell K, Coscoy L. Ubiquitination on nonlysine residues by a viral E3 ubiquitin ligase. *Science*. 2005:309(5731):127–130. https://doi.org/10.1126/science.1110340

Chen X-L, Xie X, Wu L, Liu C, Zeng L, Zhou X, Luo F, Wang G-L, Liu W. Proteomic analysis of ubiquitinated proteins in rice (Oryza sativa) after treatment with pathogen-associated molecular pattern (PAMP) elicitors. *Front Plant Sci*. 2018:9:1064. https://doi.org/10.3389/fpls.2018.01064

Chico JM, Lechner E, Fernandez-Barbero G, Canibano E, García-Casado G, Franco-Zorrilla JM, Hammann P, Zamarreño AM, García-Mina JM, Rubio V, et al. CUL3BPM E3 ubiquitin ligases regulate MYC2, MYC3, and MYC4 stability and JA responses. *Proc Natl Acad Sci U S A*. 2020:117(11):6205–6215. https://doi.org/10.1073/pnas.1912199117

Ciechanover A. N-terminal ubiquitination: more protein substrates join in. *Trends Cell Biol*. 2004:14(3):103–106. https://doi.org/10.1016/j.tcb.2004.01.004

Clark NM, Nolan TM, Wang P, Song G, Montes C, Valentine CT, Guo H, Sozzani R, Yin Y, Walley JW. Integrated omics networks reveal the temporal signaling events of brassinosteroid response in Arabidopsis. *Nat Commun*. 2021:12(1):5858. https://doi.org/10.1038/s41467-021-26165-3

Clough SJ, Bent AF. Floral dip: a simplified method for Agrobacterium-mediated transformation of *Arabidopsis thaliana*. *Plant J*. 1998:16(6):735–743. https://doi.org/10.1046/j.1365-313x.1998.00343.x

DeLong ER, DeLong DM, Clarke-Pearson DL. Comparing the areas under two or more correlated receiver operating characteristic curves: a nonparametric approach. *Biometrics*. 1988:44(3):837–845. https://doi.org/10.2307/2531595

Dey KK, Xie D, Stephens M. A new sequence logo plot to highlight enrichment and depletion. *BMC Bioinformatics*. 2018:19(1):473. https://doi.org/10.1186/s12859-018-2489-3

Dreher KA, Brown J, Saw RE, Callis J. The Arabidopsis Aux/IAA protein family has diversified in degradation and auxin responsiveness. *Plant Cell*. 2006:18(3):699–714. https://doi.org/10.1105/tpc.105.039172

Fulzele A, Bennett EJ. Ubiquitin diGLY proteomics as an approach to identify and quantify the ubiquitin-modified proteome. *Methods Mol Biol*. 2018:1844:363–384. https://doi.org/10.1007/978-1-4939-8706-1_23

Gilkerson J, Kelley DR, Tam R, Estelle M, Callis J. Lysine residues are not required for proteasome-mediated proteolysis of the auxin/indole acidic acid protein IAA1. *Plant Physiol*. 2015:168(2):708–720. https://doi.org/10.1104/pp.15.00402

Gilkerson J, Tam R, Zhang A, Dreher K, Callis J. Cycloheximide assays to measure protein degradation in vivo in plants. *Bio Protoc*. 2016:6(17):e1919. https://doi.org/10.21769/BioProtoc.1919

Gladman NP, Marshall RS, Lee K-H, Vierstra RD. The proteasome stress regulon is controlled by a pair of NAC transcription factors in Arabidopsis. *Plant Cell*. 2016:28(6):1279–1296. https://doi.org/10.1105/tpc.15.01022

Grubb LE, Derbyshire P, Dunning KE, Zipfel C, Menke FLH, Monaghan J. Large-scale identification of ubiquitination sites on membrane-associated proteins in *Arabidopsis thaliana* seedlings. *Plant Physiol*. 2021:185(4):1483–1488. https://doi.org/10.1093/plphys/kiab023

Hains PG, Robinson PJ. The impact of commonly used alkylating agents on artifactual peptide modification. *J Proteome Res*. 2017:16(9):3443–3447. https://doi.org/10.1021/acs.jproteome.7b00022

He D, Li M, Damaris RN, Bu C, Xue J, Yang P. Quantitative ubiquitylomics approach for characterizing the dynamic change and extensive modulation of ubiquitylation in rice seed germination. *Plant J*. 2020:101(6):1430–1447. https://doi.org/10.1111/tpj.14593

Igawa T, Fujiwara M, Takahashi H, Sawasaki T, Endo Y, Seki M, Shinozaki K, Fukao Y, Yanagawa Y. Isolation and identification of ubiquitin-related proteins from Arabidopsis seedlings. *J Exp Bot*. 2009:60(11):3067–3073. https://doi.org/10.1093/jxb/erp134

Kelley DR. E3 ubiquitin ligases: key regulators of hormone signaling in plants. *Mol Cell Proteomics*. 2018:17(6):1047–1054. https://doi.org/10.1074/mcp.MR117.000476

Kelley DR, Estelle M. Ubiquitin-mediated control of plant hormone signaling. *Plant Physiol*. 2012:160(1):47–55. https://doi.org/10.1104/pp.112.200527

Kim D-Y, Scalf M, Smith LM, Vierstra RD. Advanced proteomic analyses yield a deep catalog of ubiquitylation targets in Arabidopsis. *Plant Cell*. 2013:25(5):1523–1540. https://doi.org/10.1105/tpc.112.108613

Kim W, Bennett EJ, Huttlin EL, Guo A, Li J, Possemato A, Sowa ME, Rad R, Rush J, Comb MJ, et al. Systematic and quantitative assessment of the ubiquitin-modified proteome. *Mol Cell*. 2011:44(2):325–340. https://doi.org/10.1016/j.molcel.2011.08.025

Kong L, Rodrigues B, Kim JH, He P, Shan L. More than an on-and-off switch: post-translational modifications of plant pattern recognition receptor complexes. *Curr Opin Plant Biol*. 2021:63:102051. https://doi.org/10.1016/j.pbi.2021.102051

Kraft E, Stone SL, Ma L, Su N, Gao Y, Lau O-S, Deng X-W, Callis J. Genome analysis and functional characterization of the E2 and RING-type E3 ligase ubiquitination enzymes of Arabidopsis. *Plant Physiol*. 2005:139(4):1597–1611. https://doi.org/10.1104/pp.105.067983

Kravtsova-Ivantsiv Y, Ciechanover A. Non-canonical ubiquitin-based signals for proteasomal degradation. *J Cell Sci*. 2012:125(3):539–548. https://doi.org/10.1242/jcs.093567

Kulak NA, Geyer PE, Mann M. Loss-less nano-fractionator for high sensitivity, high coverage proteomics. *Mol Cell Proteomics*. 2017:16(4):694–705. https://doi.org/10.1074/mcp.O116.065136

Laussmann MA, Passante E, Düssmann H, Rauen JA, Würstle ML, Delgado ME, Devocelle M, Prehn JHM, Rehm M. Proteasome inhibition can induce an autophagy-dependent apical activation of caspase-8. *Cell Death Differ*. 2011:18(10):1584–1597. https://doi.org/10.1038/cdd.2011.27

Lee C-M, Feke A, Li M-W, Adamchek C, Webb K, Pruneda-Paz J, Bennett EJ, Kay SA, Gendron JM. Decoys untangle complicated redundancy and reveal targets of circadian clock F-box proteins. *Plant Physiol*. 2018:177(3):1170–1186. https://doi.org/10.1104/pp.18.00331

Li J, Witten DM, Johnstone IM, Tibshirani R. Normalization, testing, and false discovery rate estimation for RNA-sequencing data. *Biostatistics*. 2012:13(3):523–538. https://doi.org/10.1093/biostatistics/kxr031

Li X-M, Chao D-Y, Wu Y, Huang X, Chen K, Cui L-G, Su L, Ye W-W, Chen H, Chen H-C, et al. Natural alleles of a proteasome α2 subunit gene contribute to thermotolerance and adaptation of African rice. *Nat Genet*. 2015:47(7):827–833. https://doi.org/10.1038/ng.3305

Liu H, Wang Q, Liu Y, Zhao X, Imaizumi T, Somers DE, Tobin EM, Lin C. Arabidopsis CRY2 and ZTL mediate blue-light regulation of the transcription factor CIB1 by distinct mechanisms. *Proc Natl Acad Sci U S A*. 2013:110(43):17582–17587. https://doi.org/10.1073/pnas.1308987110

Liu H, Yu X, Li K, Klejnot J, Yang H, Lisiero D, Lin C. Photoexcited CRY2 interacts with CIB1 to regulate transcription and floral initiation in Arabidopsis. *Science*. 2008:322(5907):1535–1539. https://doi.org/10.1126/science.1163927

Ma X, Zhang C, Kim DY, Huang Y, Chatt E, He P, Vierstra RD, Shan L. Ubiquitylome analysis reveals a central role for the ubiquitin-proteasome system in plant innate immunity. *Plant Physiol.* 2021:185(4):1943–1965. https://doi.org/10.1093/plphys/kiab011

Manzano C, Abraham Z, López-Torrejón G, Del Pozo JC. Identification of ubiquitinated proteins in Arabidopsis. *Plant Mol Biol.* 2008:68(1–2):145–158. https://doi.org/10.1007/s11103-008-9358-9

Maor R, Jones A, Nühse TS, Studholme DJ, Peck SC, Shirasu K. Multidimensional protein identification technology (MudPIT) analysis of ubiquitinated proteins in plants. *Mol Cell Proteomics.* 2007:6(4):601–610. https://doi.org/10.1074/mcp.M600408-MCP200

Marshall RS, Li F, Gemperline DC, Book AJ, Vierstra RD. Autophagic degradation of the 26S proteasome is mediated by the dual ATG8/ubiquitin receptor RPN10 in *Arabidopsis*. *Mol Cell.* 2015:58(6):1053–1066. https://doi.org/10.1016/j.molcel.2015.04.023

McAlister GC, Huttlin EL, Haas W, Ting L, Jedrychowski MP, Rogers JC, Kuhn K, Pike I, Grothe RA, Blethrow JD, et al. Increasing the multiplexing capacity of TMTs using reporter ion isotopologues with isobaric masses. *Anal Chem.* 2012:84(17):7469–7478. https://doi.org/10.1021/ac301572t

Mérai Z, Chumak N, García-Aguilar M, Hsieh T-F, Nishimura T, Schoft VK, Bindics J, Ślusarz L, Arnoux S, Opravil S, et al. The AAA-ATPase molecular chaperone Cdc48/p97 disassembles sumoylated centromeres, decondenses heterochromatin, and activates ribosomal RNA genes. *Proc Natl Acad Sci U S A.* 2014:111(45):16166–16171. https://doi.org/10.1073/pnas.1418564111

Mi H, Muruganujan A, Ebert D, Huang X, Thomas PD. PANTHER version 14: more genomes, a new PANTHER GO-slim and improvements in enrichment analysis tools. *Nucleic Acids Res.* 2019:47(D1):D419–D426. https://doi.org/10.1093/nar/gky1038

Müller T, Winter D. Systematic evaluation of protein reduction and alkylation reveals massive unspecific side effects by iodine-containing reagents. *Mol Cell Proteomics.* 2017:16(7):1173–1187. https://doi.org/10.1074/mcp.M116.064048

Nielsen ML, Vermeulen M, Bonaldi T, Cox J, Moroder L, Mann M. Iodoacetamide-induced artifact mimics ubiquitination in mass spectrometry. *Nat Methods.* 2008:5(6):459–460. https://doi.org/10.1038/nmeth0608-459

Pandey UB, Nie Z, Batlevi Y, McCray BA, Ritson GP, Nedelsky NB, Schwartz SL, DiProspero NA, Knight MA, Schuldiner O, et al. HDAC6 rescues neurodegeneration and provides an essential link between autophagy and the UPS. *Nature.* 2007:447(7146):860–864. https://doi.org/10.1038/nature05853

Plubell DL, Wilmarth PA, Zhao Y, Fenton AM, Minnier J, Reddy AP, Klimek J, Yang X, David LL, Pamir N. Extended multiplexing of tandem mass tags (TMT) labeling reveals age and high fat diet specific proteome changes in mouse epididymal adipose tissue. *Mol Cell Proteomics.* 2017:16(5):873–890. https://doi.org/10.1074/mcp.M116.065524

Pramanik D, Shelake RM, Kim MJ, Kim J-Y. CRISPR-Mediated Engineering across the central dogma in plant biology for basic research and crop improvement. *Mol Plant.* 2021:14(1):127–150. https://doi.org/10.1016/j.molp.2020.11.002

Pruneda-Paz JL, Breton G, Nagel DH, Kang SE, Bonaldi K, Doherty CJ, Ravelo S, Galli M, Ecker JR, Kay SA. A genome-scale resource for the functional characterization of Arabidopsis transcription factors. *Cell Rep.* 2014:8(2):622–632. https://doi.org/10.1016/j.celrep.2014.06.033

Romero-Barrios N, Vert G. Proteasome-independent functions of lysine-63 polyubiquitination in plants. *New Phytol.* 2018:217(3):995–1011. https://doi.org/10.1111/nph.14915

Rose CM, Isasa M, Ordureau A, Prado MA, Beausoleil SA, Jedrychowski MP, Finley DJ, Harper JW, Gygi SP. Highly multiplexed quantitative mass spectrometry analysis of ubiquitylomes. *Cell Syst.* 2016:3(4):395–403.e4. https://doi.org/10.1016/j.cels.2016.08.009

Sadanandom A, Bailey M, Ewan R, Lee J, Nelis S. The ubiquitin–proteasome system: central modifier of plant signalling. *New Phytol.* 2012:196(1):13–28. https://doi.org/10.1111/j.1469-8137.2012.04266.x

Sankar A, Mohammad F, Sundaramurthy AK, Wang H, Lerdrup M, Tatar T, Helin K. Histone editing elucidates the functional roles of H3K27 methylation and acetylation in mammals. *Nat Genet.* 2022:54(6):754–760. https://doi.org/10.1038/s41588-022-01091-2

Santner A, Estelle M. The ubiquitin-proteasome system regulates plant hormone signaling. *Plant J.* 2010:61(6):1029–1040. https://doi.org/10.1111/j.1365-313X.2010.04112.x

Saracco SA, Hansson M, Scalf M, Walker JM, Smith LM, Vierstra RD. Tandem affinity purification and mass spectrometric analysis of ubiquitylated proteins in Arabidopsis. *Plant J.* 2009:59(2):344–358. https://doi.org/10.1111/j.1365-313X.2009.03862.x

Shannon P, Markiel A, Ozier O, Baliga NS, Wang JT, Ramage D, Amin N, Schwikowski B, Ideker T. Cytoscape: a software environment for integrated models of biomolecular interaction networks. *Genome Res.* 2003:13(11):2498–2504. https://doi.org/10.1101/gr.1239303

Song G, Hsu PY, Walley JW. Assessment and refinement of sample preparation methods for deep and quantitative plant proteome profiling. *Proteomics.* 2018:18(17):e1800220. https://doi.org/10.1002/pmic.201800220

Song G, Montes C, Walley JW. Quantitative profiling of protein abundance and phosphorylation state in plant tissues using tandem mass tags. *Methods Mol Biol.* 2020:2139:147–156. https://doi.org/10.1007/978-1-0716-0528-8_11

Sun Z, Xiao W, Li N, Chang L, Xu P, Li Y. Large-scale profiling of unexpected tryptic cleaved sites at ubiquitinated lysines. *J Proteome Res.* 2023:22(4):1245–1254. https://doi.org/10.1021/acs.jproteome.2c00748

Tal L, Gil MXA, Guercio AM, Shabek N. Structural aspects of plant hormone signal perception and regulation by ubiquitin ligases. *Plant Physiol.* 2020:182(4):1537–1544. https://doi.org/10.1104/pp.19.01282

Udeshi ND, Mani DC, Satpathy S, Fereshetian S, Gasser JA, Svinkina T, Olive ME, Ebert BL, Mertins P, Carr SA. Rapid and deep-scale ubiquitylation profiling for biology and translational research. *Nat Commun.* 2020:11(1):359. https://doi.org/10.1038/s41467-019-14175-1

Udeshi ND, Mani DR, Eisenhaure T, Mertins P, Jaffe JD, Clauser KR, Hacohen N, Carr SA. Methods for quantification of in vivo changes in protein ubiquitination following proteasome and deubiquitinase inhibition. *Mol Cell Proteomics.* 2012:11(5):148–159. https://doi.org/10.1074/mcp.M111.016857

Varshavsky A. Naming a targeting signal. *Cell.* 1991:64(1):13–15. https://doi.org/10.1016/0092-8674(91)90202-A

Vierstra RD. The ubiquitin–26S proteasome system at the nexus of plant biology. *Nat Rev Mol Cell Biol.* 2009:10(6):385–397. https://doi.org/10.1038/nrm2688

Vierstra RD. The expanding universe of ubiquitin and ubiquitin-like modifiers. *Plant Physiol.* 2012:160(1):2–14. https://doi.org/10.1104/pp.112.200667

Vissenberg K, Claeijs N, Balcerowicz D, Schoenaers S. Hormonal regulation of root hair growth and responses to the environment in Arabidopsis. *J Exp Bot.* 2020:71(8):2412–2427. https://doi.org/10.1093/jxb/eraa048

Wagih O. Ggseqlogo: a versatile R package for drawing sequence logos. *Bioinformatics*. 2017:33(22):3645–3647. https://doi.org/10.1093/bioinformatics/btx469

Walton A, Stes E, Cybulski N, Bel MV, Iñigo S, Durand AN, Timmerman E, Heyman J, Pauwels L, Veylder LD, et al. It's time for some "site"-seeing: novel tools to monitor the ubiquitin landscape in *Arabidopsis thaliana*. *Plant Cell*. 2016:28(1):6–16. https://doi.org/10.1105/tpc.15.00878

Wang S, Cai Y, Cheng J, Li W, Liu Y, Yang H. Motifer: an integrated web software for identification and visualization of protein post-translational modification motifs. *Proteomics*. 2019a:19(23):1900245. https://doi.org/10.1002/pmic.201900245

Wang Y-F, Chao Q, Li Z, Lu T-C, Zheng H-Y, Zhao C-F, Shen Z, Li X-H, Wang B-C. Large-scale identification and time-course quantification of ubiquitylation events during maize seedling de-etiolation. *Genomics Proteomics Bioinformatics*. 2019b:17(6):603–622. https://doi.org/10.1016/j.gpb.2018.05.005

Wang Z, Orosa-Puente B, Nomoto M, Grey H, Potuschak T, Matsuura T, Mori IC, Tada Y, Genschik P, Spoel SH. Proteasome-associated ubiquitin ligase relays target plant hormone-specific transcriptional activators. *Sci Adv*. 2022:8(42):eabn4466. https://doi.org/10.1126/sciadv.abn4466

Wei C, Wang C, Jia M, Guo H-X, Luo P-Y, Wang M-G, Zhu J-K, Zhang H. Efficient generation of homozygous substitutions in rice in one generation utilizing an rABE8e base editor. *J Integr Plant Biol*. 2021:63(9):1595–1599. https://doi.org/10.1111/jipb.13089

Winkler M, Niemeyer M, Hellmuth A, Janitza P, Christ G, Samodelov SL, Wilde V, Majovsky P, Trujillo M, Zurbriggen MD, et al. Variation in auxin sensing guides AUX/IAA transcriptional repressor ubiquitylation and destruction. *Nat Commun*. 2017:8(1):15706. https://doi.org/10.1038/ncomms15706

Xie X, Kang H, Liu W, Wang G-L. Comprehensive profiling of the rice ubiquitome reveals the significance of lysine ubiquitination in young leaves. *J Proteome Res*. 2015:14(5):2017–2025. https://doi.org/10.1021/pr5009724

Yilmaz A, Nishiyama MY, Fuentes BG, Souza GM, Janies D, Gray J, Grotewold E. GRASSIUS: a platform for comparative regulatory genomics across the grasses. *Plant Physiol*. 2009:149(1):171–180. https://doi.org/10.1104/pp.108.128579

Zhang N, Zhang L, Shi C, Tian Q, Lv G, Wang Y, Cui D, Chen F. Comprehensive profiling of lysine ubiquitome reveals diverse functions of lysine ubiquitination in common wheat. *Sci Rep*. 2017:7(1):13601. https://doi.org/10.1038/s41598-017-13992-y

Zhang X. The AIP2 E3 ligase acts as a novel negative regulator of ABA signaling by promoting ABI3 degradation. *Genes Dev*. 2005:19(13):1532–1543. https://doi.org/10.1101/gad.1318705